Preparation and Corrosion Resistance of $NiFe_2O_4$-$NiCr_2O_4$ Composite Ceramic-Based Inert Anodes

Jing Li[1], Shengzhong Bao[2], Menghan Shi[3], Changlin Li[4] and Lifen Luo[5]
1, 3. Intermediate Engineers
5. Senior Engineer
2, 4. Professor level Senior Engineers
Zhengzhou Non-ferrous Metals Research Institute of Chalco (ZRI), Zhengzhou, China
Corresponding author: sz_bao@chinalco.com.cn
https://doi.org/10.71659/icsoba2025-el001

Abstract

The new aluminum electrolysis technology with inert anodes and TiB_2 wettable cathodes is one of the important pathways for the aluminum electrolysis industry to achieve its carbon neutrality goals. The $NiFe_2O_4$-based cermet inert anodes have obvious comprehensive performance advantages. However, improving its corrosion resistance while balancing electrical conductivity and thermal shock resistance remains one of the main research directions at present. In this paper, Cr_2O_3 was introduced to prepare a $NiFe_2O_4$-$NiCr_2O_4$ composite ceramic, which was then fabricated into a cermet inert anode. Subsequently, static corrosion tests and 20 A electrolysis tests were conducted. The results showed that the corrosion resistance of the $NiFe_2O_4$-$NiCr_2O_4$ composite ceramic inert anode has significantly improved compared with the cermet inert anode based on traditional pure $NiFe_2O_4$ ceramic. Moreover, a stable and protective film layer could be formed during the electrolysis process under powered conditions.

Keywords: Inert anode, $NiFe_2O_4$-$NiCr_2O_4$ composite ceramics, $NiFe_2O_4$-based cermet, Corrosion resistance.

1. Introduction

Aluminum electrolysis technology with inert anodes can fundamentally address the issue of the release of CO_2, PFC, and CO_2 gases from the consumption of traditional carbon anodes during electrolysis. Particularly, $NiFe_2O_4$-based cermet integrates the corrosion resistance of the ceramic phase and the electrical conductivity of the metallic phase based on spinel-type ceramic materials by incorporating the metallic phase to improve the brittleness and electrical conductivity. In recent years, $NiFe_2O_4$-based cermet has been recognized as the most promising inert electrode material system. However, under the molten salt electrolysis conditions in the aluminum electrolysis (960 °C, Na_3AlF_6-Al_2O_3 molten salt), gradual corrosion of the anode materials and selective dissolution of some metallic elements are still critical problems limiting its life [1].

In recent years, significant progress has been made in the research of inert electrode materials for aluminum electrolysis, and material preparation has also scaled up from small-scale laboratory research to medium- and large-scale industrial application research [2–5]. Since Alcoa announced that a 17 % Cu-42.91 % NiO-40.09 % Fe_2O_3 inert anode (referred to as 5324-17Cu) features good electrical conductivity and corrosion resistance [6], M/$NiFe_2O_4$-based cermet has been regarded as the most promising inert anode material. Cermet with a ceramic phase of $NiFe_2O_4$ + 10NiO and a metallic phase M of binary or ternary alloy primarily composed of Cu, Ni, and Fe has been extensively studied. Research on cermet-based anode materials mainly focuses on the following aspects: first, enhancing the density of the material by optimizing sintering preparation processes; second, enhancing the corrosion resistance and electrical conductivity of the material by optimizing ceramic phase and metallic phase; third, conducting theoretical research from aspects such as electrical conductivity and corrosion mechanisms. With respect to optimization of ceramic

phase, the primary research direction involves introducing a secondary ceramic phase or oxide addition and conducting electrolytic corrosion test to investigate the changes in the phase structure and composition of the material and evaluate their effects on sintering densification, strength, microstructure, electrical conductivity, corrosion resistance, thermal shock resistance, etc., so as to identify the optimal secondary ceramic phase or added oxides and their content. NiO, TiN, ZrB_2, REO, CoO, MnO, SnO_2, V_2O_5, ZrO_2 and the like have all been used as additives [7–16].

Cr, characterized by excellent corrosion resistance, can form a thin and dense oxide film in an oxidation environment, with self-repairability. This study focuses on the ceramic phase. By introducing the secondary ceramic phase $NiCr_2O_4$ into the traditional $NiFe_2O_4$, the original $NiFe_2O_4$ single-phase ceramic is optimized into a $NiFe_2O_4$-$NiCr_2O_4$ composite ceramic. In addition, the influence of this optimization on the corrosion resistance of anode material is investigated. The experiment adopted a two-step sintering process to prepare $NiFe_2O_4$-$NiCr_2O_4$ composite ceramic, and a cold-pressing sintering process to prepare the inert anode materials required for the experiment to investigate the influence of the introduction of the secondary phase $NiCr_2O_4$ on the sintering performance, microstructure and film-forming property under electrolysis in low-temperature bath of (Cu-Ni-Fe)-$NiFe_2O_4$-based cermet, with the aim of improving the performance of inert anode materials for aluminum electrolysis.

2. Methodology

2.1 Sample Preparation

Raw materials used in the experiment: NiO, Fe_2O_3, Cu, Ni, and Cr_2O_3 were analytically pure. A two-step sintering process was adopted for the preparation of $NiFe_2O_4$-$NiCr_2O_4$ composite ceramic. First, $NiFe_2O_4$-$NiCr_2O_4$ composite ceramic raw material powder was pre-synthesized via a high-temperature solid-phase synthesis method. The synthesized powder was mixed with a binder, ball-milled, dried, molded under pressure, and then sintered into bulk materials for use in static chemical corrosion and electrolysis experiments. First, NiO, Fe_2O_3, and Cr_2O_3 were weighed in a molar ratio of 1:0.8:0.2, respectively, and mixed uniformly using a ball mill, with deionized water as the grinding medium. The mixture was dried in an oven, crushed, and sieved. After the obtained mixed powder was placed in a corundum crucible and calcined at 1000 ℃ under an air atmosphere for 6 hours in a muffle furnace, 80 %$NiFe_2O_4$-20 %$NiCr_2O_4$ceramic powder was obtained. The synthesized powder was crushed, mixed with deionized water as a dispersant, 1.5 % PVA as a binder, and ball-milled. The dried powder was molded into ⌀ 45 mm × 0.5 mm circular green blocks on the four-column hydraulic press under a pressure of 200 MPa. The green blocks were sintered at 1250 ℃ under an air atmosphere for 4 h. The sintered samples were subject to performance testing and static corrosion experiments. The synthesized metal powder and the composite ceramic product were mixed in a mass fraction of 3:7 to prepare the (Cu52Ni30Fe18) and (80 % $NiFe_2O_4$-20 % $NiCr_2O_4$-10NiO) cermet mixed powder, mixed with deionized water as a dispersant, and 1.5 %PVA as a binder, and ball-milled. The dried powder was molded into 75 × 48 ×10 mm green blocks under a pressure of 200 MPa. The green blocks were sintered at 1250 ℃ under N_2 atmosphere for 4 h to obtain electrolysis experiment samples. The sintered samples were subject to performance testing and 20 A electrolysis experiment for corrosion resistance testing. Simultaneously, pure $NiFe_2O_4$ and 30(Cu52Ni30Fe18)-70$NiFe_2O_4$ samples were prepared for contrast experiments.

2.2 Static Chemical Corrosion Experiment

The chemical corrosion experiment used a low-temperature electrolyte mainly composed of NaF-KF-AlF_3. The experimental temperature was set at 800 ℃. Circular sintered samples were immersed in the electrolyte which was placed in an alumina crucible with fixed capacity for 24 h

static corrosion. At the end of the experiment, the content of Cu, Ni, Fe and Cr in the bath was analyzed to evaluate the chemical corrosion of the samples in the electrolyte based on the content of impurities in the electrolyte.

2.3 Electrolysis Experiment

The electrolysis experiment used a low-temperature bath system mainly composed of NaF-KF-AlF_3 with cryolite ratio of 1.42. The electrolysis temperature was set at 800 °C, the mass fraction of added Al_2O_3 was 5 %, the current intensity was 20 A, the anode current density was set at 0.5 A/cm^2, and the cathodes were uniformly made of hot-pressed TiB_2 material. The schematic diagram of the electrolysis experimental setup is shown in Figure 1. At the beginning of the experiment, electrodes and accessory devices were installed as per the design. During the heating process, electrodes were lifted and suspended above the bath for heating together with the bath. After complete melting of the bath, the electrodes were lowered to the set position based on the set current density and immersed to a certain height in the bath. Then, a 20 A direct current was applied for 24 h electrolysis experiment. At the end of the experiment, electrodes were lifted above the bath level for cooling together with the calciner. After the calciner cooled down to room temperature, crucible and electrodes were removed. Aluminum balls generated from electrolysis in the bath were collected, cleaned of residual bath on the surface, and weighed to obtain the mass of the aluminum products obtained from this electrolysis test. The current efficiency of the test was calculated based on the following equation:

$$C_E = \frac{W_{act}}{0.3356It} \tag{1}$$

where:

W_{act} indicates the mass of aluminum products from the electrolysis test,
g 0.3356 indicates the electrochemical equivalent of aluminum, g/A·h,
I indicates the electrolysis current, A,
t indicates the electrolysis time, h.

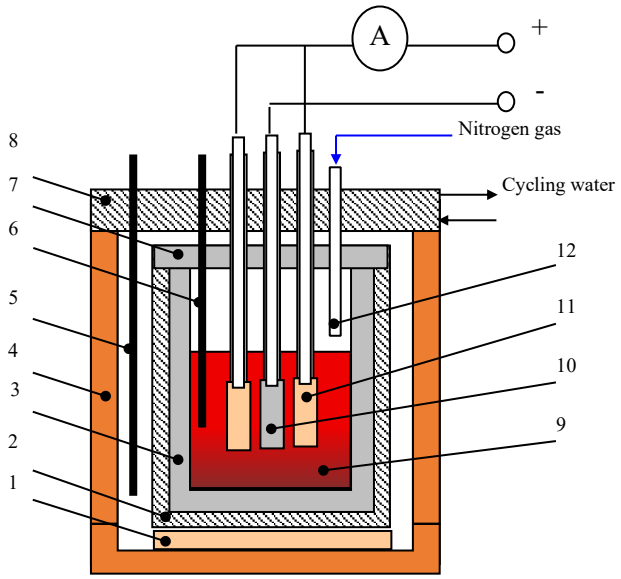

Figure 1. Schematic diagram of electrolysis experimental setup. 1-Refractory bricks; 2-Stainless steel crucible; 3-Corundum crucible; 4-Electric furnace tube; 5-Temperature-controlled thermocouple; 6-Temperature measurement thermocouple; 7 - Crucible lid; 8-Furnace roof (with cycling water cooling); 9-Molten bath; 10-Cathode; 11-Anode; 12-Nitrogen gas pipeline.

2.4 Performance Characteristics

The phase composition of the composite ceramic after high-temperature solid-phase synthesis was analyzed via XRD, and the microstructure and EDS energy spectrum of sintered and electrolyzed samples were analyzed using a scanning electron microscope (SEM); The impurity content in molten aluminium and electrolyte was analyzed using the DLS-III type ICP-OES.

3. Results and Analysis

3.1 Preparation of $NiFe_2O_4$-$NiCr_2O_4$ Composite Ceramic Powder

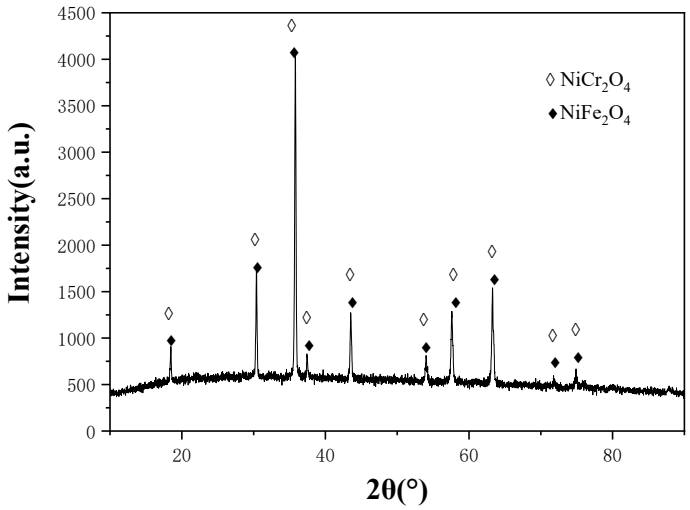

Figure 2. Phase analysis of the synthesized $NiFe_2O_4$-$NiCr_2O_4$ composite ceramic powder via XRD.

After the solid-phase synthesis reaction, the synthesized powder was taken for phase analysis via XRD. From the XRD analysis results, it can be seen that the synthesized powder is a composite oxide containing two types of spinels, $NiFe_2O_4$ and $NiCr_2O_4$. Relatively high diffraction peak intensity indicates that the synthesized product is a $NiFe_2O_4$-$NiCr_2O_4$ composite ceramic powder material with relatively high purity.

3.2 Preparation of $NiFe_2O_4$-$NiCr_2O_4$ Composite Ceramic and Cermet Materials after Incorporation of Metallic Phase

After the $NiFe_2O_4$-$NiCr_2O_4$ composite ceramic was sintered, from a macroscopic perspective, the sample surface was smooth and flat with no visible defects. SEM analysis was conducted on the sintered samples. Figure 3 shows the morphology of sintered $NiFe_2O_4$-$NiCr_2O_4$ composite ceramic, and Figure 4 shows the morphology of sintered cermet with 30 % metallic phase incorporated into the composite ceramic. It can be seen from Figure 3 that for the sintered $NiFe_2O_4$-$NiCr_2O_4$ composite ceramic, the grains are fine and dense, and fusing with each other with metallurgical bonding, free of obvious porosity or cracks overall. In the backscattered electron (BSE) mode, the crystal composition is homogeneous. Combined with the XRD spectrum of the product from the first step of synthesis in Section 2.1, it can be inferred that after secondary sintering, these two oxides are mixed with solid-solution formation of $NiFe_2O_4$-$NiCr_2O_4$ composite ceramic. After incorporation of metallic phase, in the BSE mode, it can be seen that the metallic phase is distributed in an island-like pattern in the ceramic phase. Subject

to EDS analysis, as shown in the table, it can be seen that the metallic phase comprises Cu, Ni, and Fe, with a small amount of Cr, while the ceramic phase mainly comprises Fe, Ni, and Cr oxides, and the Cr element is mainly distributed in the ceramic phase.

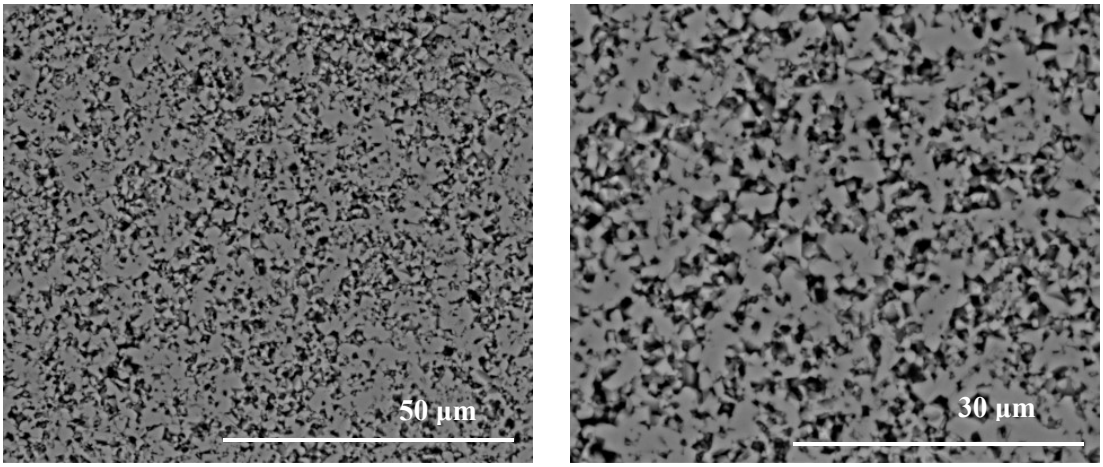

Figure 3. Morphology of sintered $NiFe_2O_4$-$NiCr_2O_4$ composite ceramic.

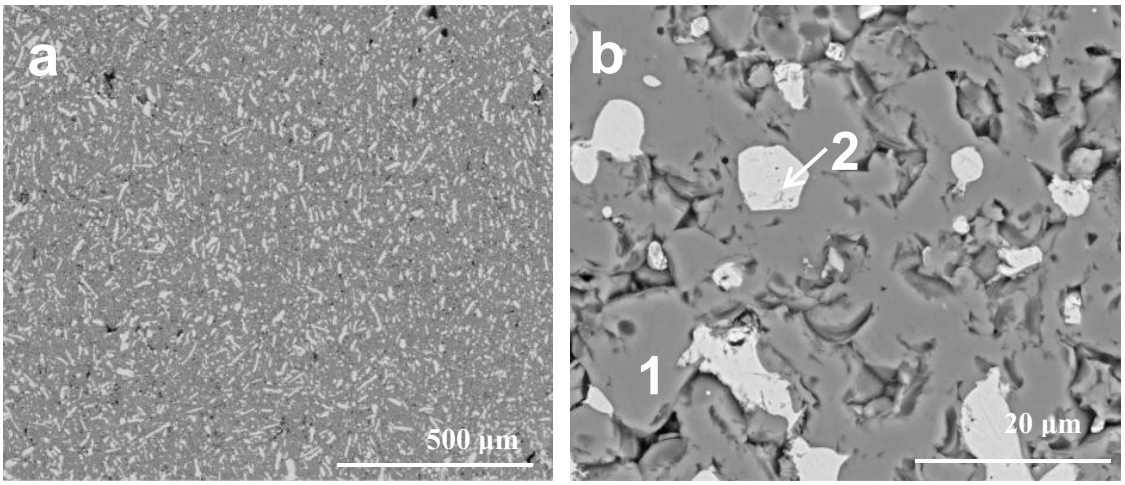

Figure 4. Morphology of sintered $NiFe_2O_4$-$NiCr_2O_4$ composite cermet.

Table 1. EDS composition analysis results of $NiFe_2O_4$-$NiCr_2O_4$ composite ceramic (At%).

Position	Cu	Ni	Fe	Cr	O
1 (metallic phase)	28.86	66	3.46	1.68	-
2 (ceramic phase)	1.33	12.22	25.77	12.83	47.84

3.3 Results and Analysis of Static Chemical Corrosion Experiment

Table 2. Impurity content in the bath after static chemical corrosion of pure ceramic phase.

Sample No.	Composition	Cu%	Ni%	Fe%	Cr%	Total/%
A	$0.2NiCr_2O_4$+$0.8NiFe_2O_4$	-	0.001	0.008	0.004	0.014
B	$NiFe_2O_4$	-	0.001	0.025	-	0.026

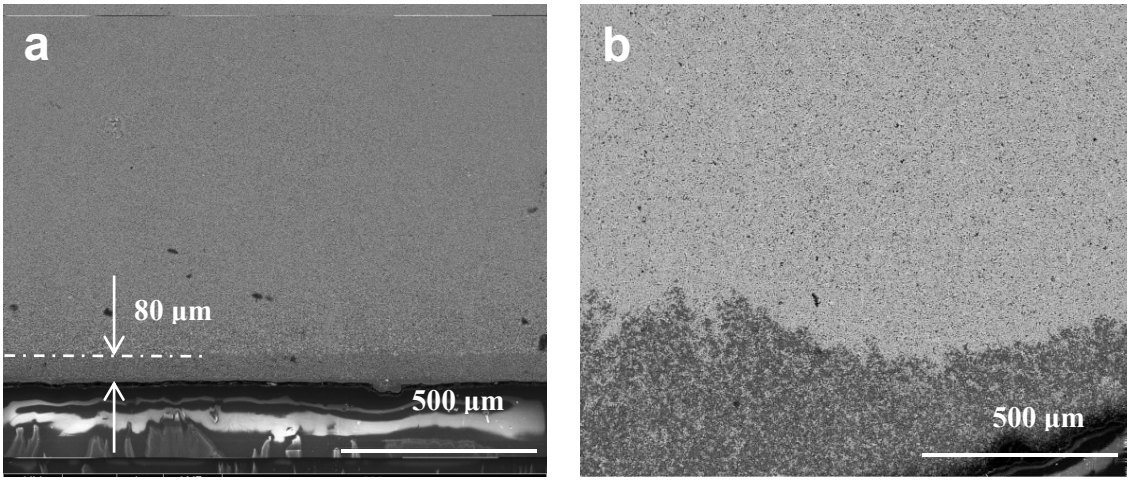

Figure 5. Film layer formed after 24 h of chemical corrosion of $NiFe_2O_4$-$NiCr_2O_4$ composite ceramic (a) and pure $NiFe_2O_4$ ceramic (b).

Static chemical corrosion experiments were conducted on $NiFe_2O_4$-$Nicr_2O_4$ composite ceramic and pure $NiFe_2O_4$ ceramic respectively. The experimental results, as shown in Table 2, show that the impurity content of $NiFe_2O_4$-$NiCr_2O_4$ composite ceramic in the bath is significantly lower than that of pure $NiFe_2O_4$ ceramic. SEM analysis of the corrosion layers of these materials further shows that after chemical corrosion of the $NiFe_2O_4$-$NiCr_2O_4$ composite ceramic, the outermost corrosion layer still maintained a closely arranged grain structure, the film layer was relatively dense and continuous, and the corrosion layer was uniform, with a thickness of only 80 μm. This indicates that the incorporation of $NiCr_2O_4$ into the ceramic phase facilitates the formation of a thinner and denser protective film layer on the material under corrosion in the bath. In contrast, the corrosion layer of pure $NiFe_2O_4$ ceramic is irregular, with obvious traces of corrosion by the bath, indicating that the material failed to form a continuous and dense oxide film layer after corrosion by the bath, and a large amount of bath penetrated into the interior of the sample. This explains the higher impurity content observed in pure $NiFe_2O_4$ ceramic. Overall, $NiFe_2O_4$-$NiCr_2O_4$ composite ceramic exhibits significantly enhanced resistance to chemical corrosion in the bath compared to pure $NiFe_2O_4$ ceramic.

To further investigate its corrosion resistance under electrolysis conditions, a cermet block was fabricated with a 70/30 ratio of $NiFe_2O_4$-$NiCr_2O_4$ composite ceramic as the ceramic phase to metallic phase and used as the anode material for electrolysis at 20 A to further examine the material's resistance to electrochemical corrosion and molten salt corrosion under powered conditions.

3.4 Results and Analysis of Electrolysis Experiment

After 24 h electrolysis experiment at 20 A, the above composite cermet, as the anode material, remained intact with no cracking or visible corrosion. In terms of microstructure (Figure 6(a)), after electrolysis, the interface of the anode material in contact with the bath is roughly divided into three layers from the outside to the inside: film layer, corrosion layer and bulk layer. EDS point analysis was conducted from the outer layer to the inner layer, and the results are shown in Table 3. Figure 6(b) shows the BSE image of the outer layer of Figure 6(a). The EDS results from different positions of the anode material show that a relatively dense film layer was formed on the outermost layer of this material, as shown at Position 1 in the figure, mainly composed of ceramic phase formed by Ni, Fe, Cu, Cr, and O, and oxides formed by $NiFe_2O_4$-$NiCr_2O_4$ and metallic phase. Position 2 is located at the corrosion layer. From the right panel, it can be seen that a relatively loose corrosion layer was formed inside the film layer. EDS results demonstrate

that K and Al ions exist in this layer, indicating that the bath has penetrated into this layer. At Positions 3 and 4, it can be seen that the bulk layer is composed of metallic and ceramic phases. According to the results of EDS analysis, the bulk layer does not contain ions from the bath, such as Al, K, Na, K, and Al, indicating that the bath has not penetrated into the bulk layer. Position 3 exhibits the metallic phase in the bulk layer containing Cu, Ni, and Fe elements, which are of the same types as the added elements, with a significant reduction of Fe content, and Position 4 exhibits the ceramic phase containing Cr, Ni, Fe, and O elements, which are consistent with the set composition. Oxygen element content in the layers of Positions 1 and 2 is higher than that in the layer of Positions 3 and 4, and there is no obvious distinction between the metallic phase and the ceramic phase in the BSE mode, indicating that under the action of the bath and the newly generated oxygen, the metallic phase in these two layers has been oxidized into the ceramic phase, forming a relatively dense protective film layer on the outermost layer, which can prevent the further inward penetration and corrosion of the bath in the subsequent experimental process and protect the inner bulk layer.

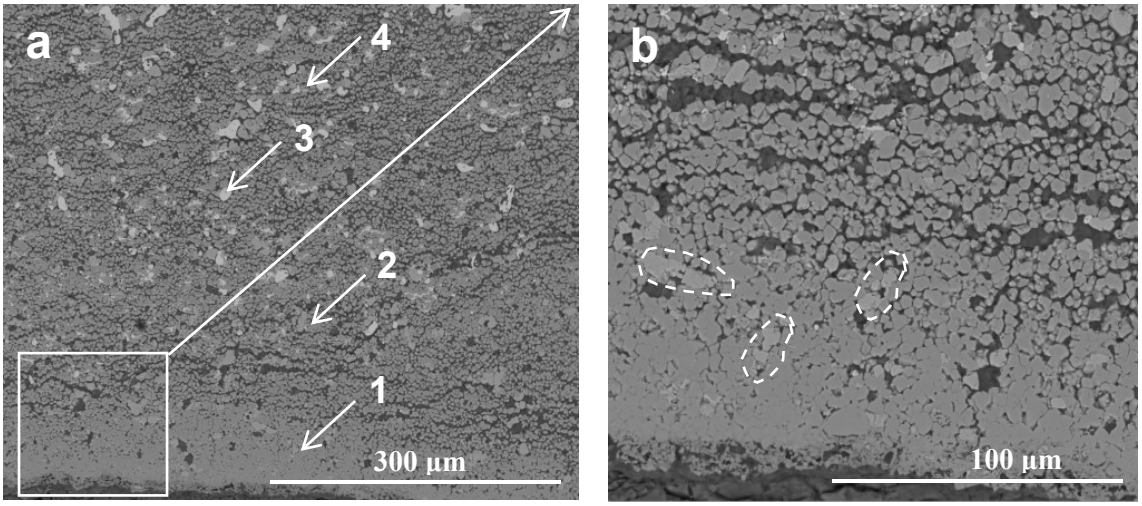

Figure 6. Film layer formed after electrolysis of $NiFe_2O_4$-$NiCr_2O_4$ composite cermet sample at 20 A (Figure (b) is an enlarged view of Figure (a)).

Table 3. EDS detection results at different points in Figure (6a) (At%).

Position	Ni	Fe	Cu	Cr	O	Al	K
1	10.87	13.96	-	8.06	67.11	-	-
2	11.42	14.06	-	7.41	60.70	4.20	2.21
3	29.20	4.03	66.77	-	-	-	-
4	22.03	23.91	-	11.46	42.59	-	-

In summary, the outermost film layer formed by the material in contact with the bath (Position 1 in Figure 6(a)) is mainly composed of ceramic phase. The color at the dotted line in Figure 6(b) is slightly different from that around it, suggesting that the metallic phase of this layer was in-situ oxidized to the ceramic phase under the combined action of the corrosion of the bath and newly generated oxygen, bonding with the original ceramic phase due to volume expansion, resulting in a relatively dense film layer. Inside the film layer lies a corrosion layer, formed by corrosion of the bath penetrating the film layer to the anode body. This layer is relatively loose and not as dense as the outermost film layer. This is attributed to the fact that the newly generated oxygen from electrolysis mainly exists on the material surface, incapable of reaching the corrosion layer, preventing rapid oxidation of the metallic phase into the ceramic phase, while K and Al ions with strong penetrability in the bath can pass through the film layer and further corrode the metallic phase, as evidenced by the lower oxygen content at Position 2 compared to Position 1 in Figure 6(a). There is still a small amount of bath penetration into the film layer, while there is no

bath penetration into the bulk layer, indicating that the formed film layer has a certain protective effect.

Overall: $NiFe_2O_4$-$NiCr_2O_4$ composite cermet can form a protective film layer in the bath, resulting from in-situ oxidation and expansion of the ceramic phase and the metallic phase. The corrosion layer formed by penetration of a small amount of electrolyte and the bulk layer without corrosion of electrolyte indicates that although a film layer has been formed, it is required to improve and enhance the resistance to corrosion of electrolyte and molten salt for the $NiFe_2O_4$-$NiCr_2O_4$ composite cermet under powered conditions.

4. Conclusion

(1) $NiFe_2O_4$-$NiCr_2O_4$ composite ceramic powder with high purity can be synthesized by mixing NiO, Fe_2O_3 and Cr_2O_3 in a molar ratio of 1:0.8:0.2 and holding the mixture at 1000 °C for 6 hours under an air atmosphere.

(2) The incorporation of $NiCr_2O_4$ phase in the ceramic phase can enhance the static corrosion resistance of $NiFe_2O_4$-based anode materials in the NaF-KF-AlF_3 low-temperature bath system, as the film layer formed on its surface is relatively dense.

(3) After the electrolysis test of $NiFe_2O_4$-$NiCr_2O_4$ composite cermet, although a complete film layer can be formed in terms of microstructure, it is necessary to improve the resistance to bath corrosion of the film layer.

5. References

1. Yong He et al., Recent progress of inert anodes for carbon-free aluminium electrolysis: a review and outlook, *Journal of Materials Chemstry A*, 2021, Issue 45, 25272-25285. https://doi.org/10.1039/d1ta07198j
2. Kaibin Chen, et al., Research Progress on Inert Anode Materials for Aluminum Electrolysis. *TMS-Light Metals* 2025, 850–857. https://doi.org/10.1007/978-3-031-80676-6_106
3. Liao Xianan et al. Review on current major carbon-free aluminum reduction technology. *Light Metals*, 2019(3):1-4 (in Chinese).
4. Kaibin Chen, et al., Research progress on inert anode materials and electrolytic technology for aluminum electrolysis, *China Nonferrous Metallurgy*, 2024, 53 (06):59–68. https://doi.org/doi:10.19612/j.cnki.cn11-5066/tf.2024.06.007 (in Chinese)
5. Sai Krishna Padamata, et al., Review primary production of aluminium with oxygen evolving anodes, *Journal of The Electrochemical Society*, 2023, 170(7): 073501. https://doi.org/10.1149/1945-7111/ace332
6. J.D. Weyand, Manufacturing processes used for the production of inert anodes, *Light Metals,* 1986, 321–339.
7. Bin Wang, et al. Sintering behavior and fracture morphology of $NiFe_2O_4$/nano-TiN ceramics synthesized under argon atmosphere, *Journal of Materials Engineering and Performance*, 2020, 29(12): 7971–7980. https://doi.org/10.1007/s11665-020-05009-z
8. Zhigang Zhang and Jianrong Xu, Sintering kinetics and properties of $NiFe_2O_4$-based ceramics inert anodes doped with TiN nanoparticles. *International Journal of Applied Ceramic Technology*, 2023, 20(1): 329-340. https://doi.org/10.1111/ijac.14231
9. Zhiyou Li, et al., A highly corrosion-resistant cermet inert anode material for aluminum electrolysis and its preparation method, *China Patent*, CN 113186569B, Submitted on July 30, 2021, Authorized on March 5, 2024 (in Chinese). https://patents.google.com/patent/CN113186569B/zh

10. Hanbing He et al., *A ZrB_2-based cermet inert anode and its preparation method and application*: China Patent, CN1159476 02B, Submitted on April 11, 2023, Authorized on March 5, 2024 (in Chinese). https://patents.google.com/patent/CN115947602A/zh
11. Yuqiang Tao et al., Conductivity and corrosion resistance of Yb_2O_3 or Y_2O_3-Doped Cu-($NiFe_2O_4$-10NiO) inert anode, *The Chinese Journal of Nonferrous Metals*, 2011, 21(5): 1137–1144 (in Chinese).
12. Haiming Wu et al., Effect of CoO doping on the conductivity of 15(20Ni-Cu)/(NiO-$NiFe_2O_4$) cermet, *Materials Science and Engineering of Powder Metallurgy*, 2011, 16(2): 206–211 (in Chinese).
13. Wei Wang et al., Effect of ceramic phase doping on the performance of inert anode materials for aluminum electrolysis. *The Chinese Journal of Nonferrous Metals*, 25(6), 1653-1658. (in Chinese).
14. Zhang Xiao,et al.,The influence of ZrO_2 on the properties of $NiFe_2O_4$-based cermet inert anodes. // *National Doctoral Academic Annual Conference.* China Association for Science and Technology; Office of the Academic Degrees Committee of the State Council, 2012. (in Chinese)
15. Lin Qiquan, et al. Effect of La_2O_3 doping on microstructure and properties of cermets. Journal of the Chinese Ceramic Society,2014,(12): 1537-1542. (in Chinese).
16. Ana-Maria Popescu, Oxygen-evolving SnO_2-based Ceramic Anodes in Aluminium Electrolysis, *Chemical Research in Chinese Universities*, 2014, Volume 30(5): 800-805. http://doi.org/10.1007/s40242-014-4137-4